ISSN 1027-4510, Journal of Surface Investigation: X-ray, Synchrotron and Neutron Techniques, 2020, Vol. 14, No. 1, pp. 66–72. © Pleiades Publishing, Ltd., 2020.
Russian Text © The Author(s), 2020, published in Poverkhnost', 2020, No. 1, pp. 81–88.

# Influence of Chromium on the Chemical Composition and Surface Properties of Rapidly Solidified Al–Cr Alloys

**I. I. Tashlykova-Bushkevich[a, *], V. G. Shepelevich[b], M. Amati[c], L. Gregoratti[c], and M. Kiskinova[c]**

[a] *Belarusian State University of Informatics and Radioelectronics, Minsk, 220013 Belarus*
[b] *Belarusian State University, Minsk, 220050 Belarus*
[c] *Elettra Sincrotrone, Trieste, 34012 Italy*
**e-mail: iya.itb@bsuir.by*

Received February 14, 2019; revised March 26, 2019; accepted March 26, 2019

**Abstract**—The microstructure and physicochemical properties of the surface of rapidly solidified Al–Cr alloys containing 1 and 3 at % of chromium are studied by means of photoelectron microscopy using synchrotron radiation, scanning probe microscopy, and the sessile-drop technique. We find that the surface oxide-hydroxide layer of foils has a heterogeneous structure with highly dispersed chromium inclusions (possibly clusters). Chromium and aluminum are predominantly in a metallic state in chromium-enriched regions of the foil surface. We find that the equilibrium contact angle of wetting of the samples with water depends on their morphology and the concentration of chromium in the alloys. The wettability is mainly determined by the chemical composition of the surface of foils and to a lesser extent its roughness. A decrease from poor to low water wettability of rapidly solidified Al–Cr alloys with an increase in the chromium concentration up to 3 at % is due to the aggregation of chromium inclusions.

*Keywords:* rapid crystallization, Al–Cr alloys, photoelectron spectroscopy, synchrotron radiation, scanning probe microscopy, wettability

**DOI:** 10.1134/S102745102001019X

## INTRODUCTION

Currently, medium-strength aluminum alloys are successfully used in the storage and transportation of compressed hydrogen fuel as an alternative to gasoline and diesel fuel. High-strength aluminum alloys are limited in use because of their susceptibility to hydrogen embrittlement during operation at elevated pressures [1–3]. Intensive works to create materials from high-strength aluminum alloys for hydrogen power engineering and reinforcing elements of hydrogen lines, therefore, are aimed at avoiding the negative effect of hydrogen on the mechanical properties of aluminum materials. Despite the advances of experimental and theoretical studies on the mechanisms and forms of hydrogen embrittlement [4–6], significant progress in studying the interaction of hydrogen with structural microdefects and macrodefects may be achieved due to new methods of analysis of the structure and chemical composition of alloys under nanoscale resolution.

Fundamental studies of the behavior of hydrogen in aluminum and its alloys require studies of the influence of physicochemical processes during crystallization on the structure and properties of aluminum alloys depending on the composition of samples, the method of their preparation, and processing conditions. The behavior of hydrogen in rapidly solidified aluminum alloys is of particular interest. Despite the fact that many alloying components of industrial aluminum alloys are poorly soluble in aluminum under equilibrium conditions, an anomalous increase in their solubility in a solid solution is achievable due to rapid crystallization [7, 8]. For example, the solubility of chromium in aluminum in binary aluminum alloys, for example, exceeds the equilibrium solubility limit by 3.4 times to reach 1.5 at % as a result of centrifugal quenching [9]. This expands the possibilities of the heat treatment of supersaturated solid solutions and allows improvement in the properties of aluminum alloys due to alloying with transition metals (chromium, iron, zirconium, titanium, and others) and rare-earth elements (scandium, yttrium, lanthanum, and others). Another feature of rapidly solidified materials is the dispergation of structural components of alloys during solidification, including the separation of dispersed inclusions of nonequilibrium intermetallic phases, whose composition and structure differ from equilibrium phases, which leads to hardening of the samples.

When the kinetics of hydrogen evolution from rapidly solidified foils of aluminum and its binary alloys with chromium and those with iron and zirconium was

studied, the authors found that the mechanism of hydrogen trapping by nonequilibrium defects in foils of aluminum alloys is qualitatively changed in comparison with samples obtained with conventional methods [10–13]. This makes it possible to control the rate of hydrogen permeation (to slow it down) through rapidly solidified materials. Modification of the structure and surface properties of aluminum alloys using methods of rapid solidification, therefore, is of fundamental and practical importance to avoid the hydrogen embrittlement of metals and their alloys that are in contact with an aggressive hydrogen-containing environment.

The aim of this work is a comprehensive study of the microstructure, composition, and chemical state of the surface of rapidly solidified Al–Cr binary alloys with scanning photoelectron microscopy (SPEM) and scanning probe microscopy (SPM) to determine the effect of the alloying element chromium on the chemical composition and properties of rapidly solidified foils. High-resolution synchrotron radiation (SR) photoelectron microscopy and SPM make it possible to determine the elemental composition and visualize the surface structure of an object at a submicroscopic level. The sessile-drop technique was used as an express and highly sensitive method for studying the physicochemical properties of the surface of the samples. Considering that the surface layer of rapidly solidified alloys is in a special physicochemical state and its properties are different from the bulk properties of a material, the degree of wettability of foils with distilled water was measured from the contact angle as a sensitive indicator of the microstructure and chemical composition of the surface of solids.

## EXPERIMENTAL

Rapidly solidified Al–Cr alloys containing 1 and 3 at % Cr were obtained via the centrifugal quenching of a melt with one-sided heat removal, when a drop of melt was splashed onto the inner surface of a copper cylinder. The cooling rate of the melt was no lower than $10^6$ K/s [14] at a rotational speed of 1500 rpm of a cylinder with a diameter of 20 cm. The thickness of the foils was 50–100 μm and the width was 5–10 mm. The foil surface in contact with air was chosen to analyze the microstructure, composition, and properties.

The microstructure and chemical composition of the Al–Cr alloy foils were studied by means of SPEM method in the 2D microscopic imaging and spectroscopic modes at the ESCA microscopy beamline in the synchrotron radiation facility ELETTRA at an electron-beam energy of the storage ring of 2.4 GeV. The photoelectrons were recorded on a PHOIBOS 100-mm hemispherical energy analyzer equipped with a 48-channel detector developed in ELETTRA [15]. The energy analyzer was installed at an angle of 60° to the direction of radiation incident normally on the surface of the samples. Electrons emitted from an extended portion of the sample surface irradiated with photons are detected in the multichannel operation mode of the analyzer, which allows one to obtain two-dimensional images of the foil containing information about the distribution of elements in various chemical states over the surface. The analyzer in the spectroscopic mode of X-ray photoelectron spectroscopy (μ-XPS) detects photoelectrons emitted from a submicron region of the surface. The photoelectron spectra of core electrons (electrons on inner shells of an atom) allow the identification of chemical elements and analysis of the chemical composition of a small area of the sample surface.

The foil surface during the SPEM experiments was irradiated with photons having an energy of $h\nu = 650$ eV. The foil was purified from excess carbon during etching of the sample surface with argon ions with an energy of 2 keV. The working vacuum in the experimental chamber of the spectrometer was $10^{-7}$ Pa. The diameter of the SR beam focused by means of the Fresnel zone plate was ~120 nm. The photon energy was calibrated from the signal of a gold film according to the position of the Fermi level and Au4$f_{7/2}$ core level. The analysis depth at a photon energy of 650 eV was several nanometers, the energy resolution was 0.3 eV, and the spatial resolution was less than 0.1 μm. Other experimental details are described elsewhere [16]. The processing of μ-XPS spectra (subtraction of the nonlinear background with the Shirley method [17] and normalization) was performed with Igor Pro software. The NIST database was used to analyze the chemical state of elements [18].

The morphology and roughness of the foil surface in contact with air were studied using SPM on an NT-206 atomic force microscope in the contact mode in air; Si standard and CSC-38 probes were used. Images 36 × 36 μm in size were processed using SurfaceXplorer software (Mikrotestmashiny, Belarus) [19]. The arithmetic average roughness $R_a$ was found from the data obtained from four to five areas selected randomly for each alloy. The relative measurement error of $R_a$ was about 3.5%.

The wettability of the samples with distilled water was found via the sessile-drop technique in air from the equilibrium contact angle θ measured by means of digital processing of the droplet profile with a volume of 50 μL on the foil surface in contact with air. The drops were placed (up to four on one foil) with the help of syringe at the equipment described in [20]. The stabilization time of the foil–distilled water system was 60 s under ~18°C. The error in measuring the equilibrium water contact angle was ~1°.

## RESULTS AND DISCUSSION

Figures 1a and 1b show the two-dimensional SPEM images of a characteristic region of the foil air-side surface of Al–1 at % Cr alloy obtained via the

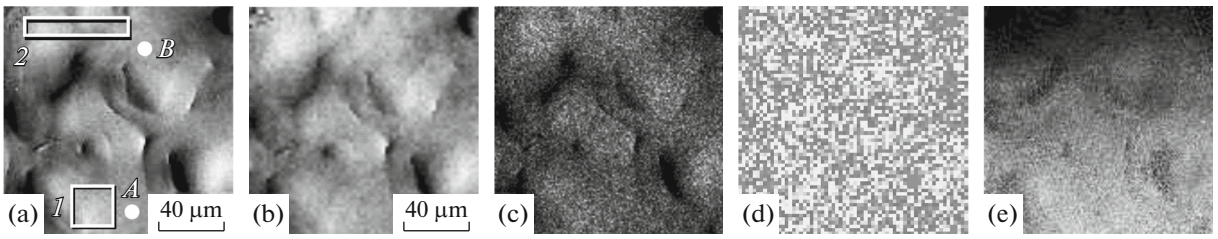


**Fig. 1.** Photoelectron mapping of rapidly solidified Al–1 at % Cr alloy foil: (a) SPEM image of Al2*p*, (b) SPEM image of Cr3*p* of a characteristic area of the foil surface, the corresponding (c) Al and (d) Cr distribution maps together with (e) distribution map of metallic Al relative to $Al_2O_3$ oxide. The size of each image is 130 × 130 $\mu m^2$.

recording of Al2*p* and Cr3*p* photoemission signals, respectively. The same features of the surface relief of the sample are dominant in both figures due to the contribution of topographic contrast. The SPEM images, therefore, were processed to remove topographic artifacts [16]. Figures 1c and 1d show the photoelectron maps of aluminum and chromium distribution over the surface of the foil: the processed SPEM images, whose compositional contrast is determined by the elemental composition of the surface region of the rapidly solidified samples. The local heterogeneity of contrast of the image (Fig. 1d) indicates that there are finely dispersed zones on the foil surface with a high concentration of chromium (possibly as clusters) and zones with a low amount of chromium. Considering that processing of the photoelectron maps allows one to study the change in the chemical composition of the samples with lateral resolution, Fig. 1e also shows a distribution map of Al in the metallic state relative to that in the oxidized one obtained after the processing of SPEM images recorded at photoelectron energies corresponding to the bond energies of metallic Al and $Al_2O_3$ oxide, respectively. Analysis indicates that there are areas on the foil surface, where aluminum is predominantly in the metallic (unoxidized) state. There is, for example, a region *1* (Fig. 1a), which visually seems to be light (Fig. 1e) in comparison with the darkened region *2* (Fig. 1a), which corresponds to the area, in which Al is mainly in the oxidized state.

Micro-XPS analysis of the foil surface of the Al–1 at % Cr alloy was performed in submicron regions designated as *A* and *B* (Fig. 1a) and in areas of a finite size of the same area (Fig. 1a, section *1* of 25 × 24 $\mu m^2$ in size and a section *2* of 60 × 10 $\mu m^2$ in size). Figure 2 shows the photoelectron spectra of Al2*p* and Cr3*p*. There are two lines in the Al2*p* spectra (Figs. 2a and 2b). The first one with a bond energy of 72.8 eV corresponds to aluminum in the metallic state and has the highest intensity in the spectra measured in regions *A* and area *1*. The second line with a peak position at 73.4–76.0 eV, which is typical for Al–O bonds, is relatively wide and shifts to the region of higher bond energies if the area of analysis is changed to region *B* and area *2*. Analysis of the 3*p* line of Cr in the range 41.6–43.5 eV (Figs. 2c and 2d) showed that there is chromium only in region *A* and area *1*, whereas it is not detected in region *B* and area *2*.

The change in the spectra of the Al2*p* level (Figs. 2a and 2b) from the region with a high amount of chromium (curves *A* and *1*) to that with a low amount of chromium (curves *B* and *2*) indicates that the low-energy component corresponding to metallic aluminum (72.8 eV) has the highest intensity in the regions enriched in chromium. $Al_2O_3$ with a bond energy of 75.7 eV is a predominant phase in regions with a low amount of chromium. This allows us to conclude that chromium inhibits the oxidation of aluminum on the surface of the foil. In addition, hydroxides also appear in the foils together with oxidized aluminum and metallic aluminum, and broadening of the Al2*p* profile at high bond energies confirms this fact. A satisfactory approximation of the photoelectron spectra of the core level of Al2*p* aluminum was obtained in previous experiments [21] for Al–3 at % Cr alloy, taking into account the formation of $Al(OH)_3$ and AlOOH hydroxides. It is difficult, however, to prove the origin of aluminum hydroxides according to μ-XPS analysis because of the complex multicomponent structure of the spectra and disagreement between the reference and literature data on the bond energies of the high-energy components of aluminum lines [18]. As a result, the phase composition of the pure aluminum foils and its alloys with chromium is additionally planned to be studied with X-ray diffraction analysis.

The Cr3*p* X-ray photoelectron spectra (Figs. 2c and 2d) demonstrate that chromium is mainly in the metallic state in the chromium-rich regions (curves *A* and *1*). It should be noted, however, that the bond energy at 41.6 eV of a low-energy component having the highest intensity and corresponding to metallic chromium is lower than the published data (41.9 [22] and 42.1 eV [23]). In addition, an unusual high-energy "oxide" peak, whose decomposition components are assigned to chromium oxides, is observed in the μ-XPS spectra (curves *A* and *1*). A comparison with the available published data on the bond energy of core Cr3*p* levels for $CrO_2$ (43.5 eV [24]) and $Cr_2O_3$ (43.9 eV [25]) shows that there is a general tendency that the signals are shifted towards lower bond energies in the Cr3*p* spectra in contrast to the Al2*p* spectra. In addi-

tion, the bond energy of the Cr2$p_{3/2}$ main peak in the spectral profiles of Cr2*p* electrons measured previously for Al–3 at % Cr alloy [21] is 574.0 eV, which is in good agreement with the published data (573.8–574.7 eV) [18]. The shape of the Cr2*p* and Cr3*p* photoelectron spectra of Al–1 at % Cr alloy and Al–3 at % Cr alloy foils indicates that chromium is insignificantly oxidized on the surface of the foil in those areas enriched in chromium (designated as *A* in Fig. 1a). This fact may be indirect evidence of the segregation of a large fraction of chromium in the surface layer of the samples into clusters, during the localization of which it interacts less actively with atmospheric oxygen and moisture.

Figure 3 shows the typical topography of the foil air-side surface of Al–Cr alloys. The surface morphology of the samples has an aperiodic grain structure with a grain size of 1–5 μm. The microrelief includes heights, cavities, and flat areas together with disordered acute-angled and obtuse-angled conical structures (Figs. 3a and 3b). The grain height above the foil surface is 100 nm in some areas. The arithmetic average surface roughness differs by 9% for Al–1 at % Cr alloy and Al–3 at % Cr alloy foils and is 39.2 and 42.7 nm, respectively. Figure 3c shows the equilibrium water contact angles for Al–Cr alloys. The inserts in Fig. 3a and 3b show the shape of distilled water droplets placed on the air-side surface of the rapidly solidified foils. We found that chromium changes the hydrophobic properties of pure aluminum foils (99.99%), which are poorly wetted with water ($\theta = 87.7°$ for the air-side surface of Al foils) [20]. When the nominal concentration of chromium increases in alloys from 1 to 3 at %, there is a decrease in the contact angle θ from 86.2° to 75.2°, respectively.

The SPEM results of the rapidly solidified Al–1 at % Cr alloy are in good agreement with those obtained previously for rapidly solidified Al–3 at % Cr alloy [21], and they make it possible to find the following regularities of the microstructure of the surface layers of foils of Al–Cr alloys. Nonequilibrium crystallization during the rapid cooling of a melt leads to oxide-hydroxide surface layers including a low amount of chromium and having an inhomogeneous structure: there are areas with high and low amounts of chromium on the foil surface. Photoelectron mapping of the surface of the foils during the recording of Cr2*p* [21] and Cr3*p* photoemission signals suggests that chromium clusters are formed on the surface of the foils. Figure 1d indicates that light shaded aggregates (agglomerates) mainly consisting of metallic chromium apparently segregated into clusters are unevenly distributed over the surface of the foil. Although it is not possible to assess the size and structure of the clusters by means of SPEM, there is a decrease in the bond energy of 3*p* core chromium electrons in the rapidly solidified Al–1 at % Cr alloy despite the fact that there is no shift in the position of the core aluminum peaks. This effect not observed in Al–3 at % Cr alloy (probably due to the aggregation of chromium precipitates) is due to an increase/decrease in bond energy of core electrons of cluster atoms compared to those in bulk samples. This makes it difficult to identify the chemical state of a material from chemical shifts of photoelectron lines in the presence of metal clusters and their oxides in the matrix [26, 27]. Numerous theoretical and experimen-

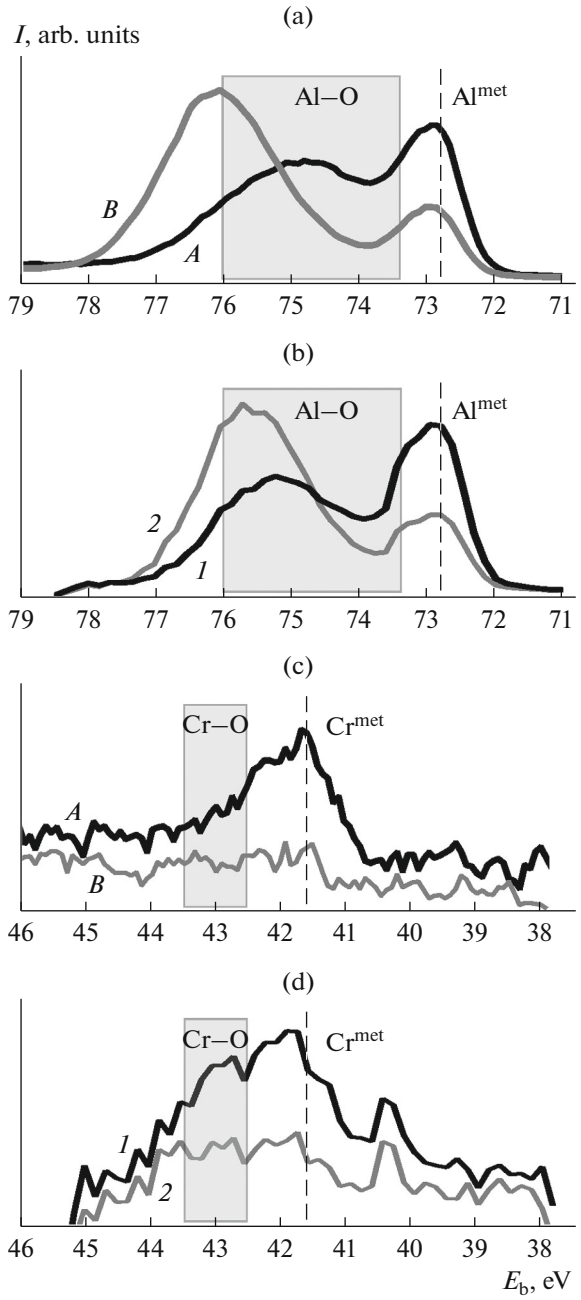


**Fig. 2.** Photoelectron spectra of: (a and b) Al2*p* and (c and d) Cr3*p* states measured for various surface regions of rapidly solidified Al–1 at % Cr alloy. Curves *A* and *B* correspond to submicron regions *A* and *B* in Fig. 1a, whereas curves *1* and *2* correspond to regions *1* and *2* of the same area of 600 $\mu m^2$ in Fig. 1a.

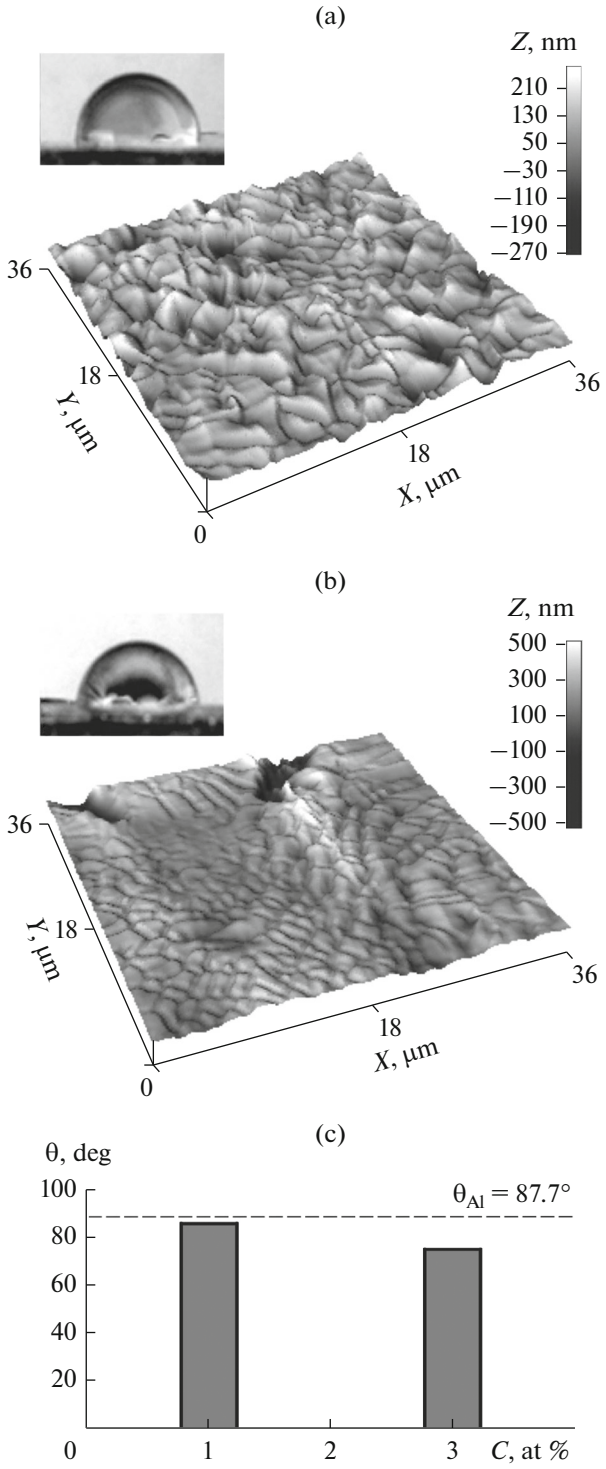


**Fig. 3.** Morphology and wettability of rapidly solidified foils of: (a) Al–1 at % Cr and (b) Al–3 at % Cr alloys, and (c) the histogram of the equilibrium water contact angle of wetting versus nominal amount of chromium in the alloys. The inserts (a) and (b) show the shape of droplets on the surface of the samples.

tal data obtained for transition and noble metals indicate that the sign and magnitude of a shift in the bond energy measured with SPEM depend on the size of clusters (from some nanometers to 100 nm and higher), the chemical state, the mutual arrangement of their atoms, and the substrate material [26, 28, 29]. It is preferable, therefore, to compare only experimental data obtained for similar samples. It is interesting to note, however, that there is an increase in the bond energy of $2p_{3/2}$ and $3p$ core levels by 0.35 and 0.45 eV, respectively, for chromium nanoclusters (with an average size of 1.5 nm) on a graphite surface [29] in comparison with those positions of $Cr2p_{3/2}$ and $Cr3p$ lines at 574.40 and 42.10 eV, respectively. In-situ SPEM analysis of the samples showed that there is no oxidation of chromium nanoclusters.

Another characteristic feature of rapidly solidified foils of Al–Cr alloys is the local suppression of aluminum oxidation in submicron regions enriched in chromium. Meanwhile, despite a different composition, different preparation conditions of samples, and oxidation methods, our experimental data are in agreement with the fact that aluminum segregates on the surface in Al–Cr alloys, whereas chromium is either mainly located below the oxide layer or it incorporated into the oxide film in the metallic state [30, 31]. Such a behavior of chromium in the surface layer of samples is probably due to the predominant oxidation of aluminum owing to the large free formation energy of its oxide, which was experimentally observed in the oxidation processes of iron–chromium–aluminum alloys [32].

The experimental increase in the degree of hydrophilicity of the foil surface during alloying aluminum with chromium within the concentration range of 1–3 at % Cr indicates that the wettability of the foils strongly correlates with the chemical composition of their surface. Indeed, the equilibrium water contact angle decreases by only 1.5° despite the fact that the roughness of the foils increases after the introduction of 1 at % of chromium ($R_a$ of aluminum air-side surface is 17 nm for areas with a size of 20 × 20 μm$^2$ [33]); in other words, the wetting properties of Al–1 at % Cr alloy negligibly differs from those of pure aluminum foils, which are poorly wetted with water (θ value is 90°). This confirms the conclusion that the surface regions of the samples contain a low amount of chromium, and metallic chromium aggregates segregate into clusters, which are unevenly distributed over the surface of the foil. An increase in the amount of chromium in the alloy up to 3 at % decreases the equilibrium water contact angle of wetting by 13% with a slight increase in roughness of the foil. As a result, an increase in the degree of hydrophilicity of the foils with an increase in the chromium concentration in the alloy is probably due to the aggregation of chromium precipitates and an increase in the amount of chromium regions with a low amount of aluminum oxide and its hydroxides despite the fact that the surface of the foils has a low amount of chromium, which leads to a decrease in the contact angle. At the same time, Al–3 at % Cr alloy

foils possess low wettability, because the angle θ remains large enough to be 75.2°. The latter is of great interest, because a contact angle of 90° between the water drop and the surface of the sample is a conditional boundary that determines the degree of its wettability with water in accordance with a general division of the materials into hydrophobic and hydrophilic. Considering that water spreads well on high-energy surfaces of materials with metallic, covalent or ionic bonds [34, 35], aluminum is expected to exhibit hydrophilic properties. Indeed, numerous experimental studies indicate [36–38] that Al samples and its alloys are well wetted with water, and the equilibrium contact angle of wetting, as a rule, is several times lower than 90° despite different preparation methods of the surface. Nevertheless, there are some data that large wetting angles θ within 70°–90° are typical of aluminum and some of its alloys during their contact with water [20, 39–41]. The authors assumed that this effect is probably due to aluminum oxides and hydroxides [42, 43] on the surface of the materials and their interaction with the atmosphere. The authors, however, noted that the role of the composition and chemical state of the surface of aluminum materials during homogeneous/heterogeneous wetting remain poorly understood.

The study of structure and physicochemical state of the surface of alloys are especially important for the development of materials used in aggressive liquid and gas environments. Currently, chromium alloying is widely used to increase the thermal stability and corrosion resistance of industrial alloys [3, 44]. As a result, the behavior of chromium in aluminum materials obtained via various technologies of both surface [45, 46] and bulk alloying is actively studied. Our results expand modern ideas about the microstructure, including the chemical and phase composition, of oxide films/oxidized surfaces of aluminum alloys and the effect of the surface on the physicochemical properties of alloys obtained via nonequilibrium crystallization. Additional studies of the evolution of structure and the properties of materials depending on the composition of samples and heat treatment are required for a more complete understanding and determination of the potential for rapid crystallization to modify the structure and properties of aluminum alloys, including for practical applications in hydrogen material science.

## CONCLUSIONS

The microstructure of rapidly solidified Al–Cr alloys was studied with photoelectron spectroscopy using SR, scanning probe microscopy, and the sessile-drop technique and the effect of chromium on the chemical composition and surface properties of the samples was investigated. Finely dispersed chromium inclusions distributed nonuniformly over the surface of the samples were found in the surface area of foils with a low amount of chromium. Chromium leads to a change in the ratio of the characteristic features of metal and oxide components in the photoelectron spectra of aluminum. The metal component of the Al2*p* core level spectra corresponding to aluminum in the metallic state is predominant in regions enriched in chromium, whereas there is an increase in the relative amount of $Al_2O_3$ oxide and aluminum hydroxides in regions with a low amount of chromium. SPM data showed that the roughness of the foils during the doping of aluminum with chromium within 1–3 at % increases slightly and is 39.2 and 42.7 nm, respectively. The relationship between the equilibrium water contact angle and the physicochemical state of the surface of rapidly solidified alloys indicates that the wettability of the foil surface is mainly determined by its chemical composition. When 3 at % chromium is introduced, the degree of hydrophilicity of the foils increases: the contact angle θ decreases by 13% up to 75.2°. We showed, therefore, that SR makes it possible to expand the capabilities of photoelectron spectroscopy and perform mapping with visualization of the distribution of elements in various chemical states over the surface of samples with a submicron spatial resolution. We also showed that the sessile-drop technique can be successfully used along with direct methods to study the structure of samples (both at submicroscale and nanoscale) for macroanalysis of structural and chemical heterogeneity of materials obtained via nonequilibrium crystallization.

## ACKNOWLEDGMENTS

We are grateful to Yu.S. Yakovenko for the assistance with SPM measurements at the Belarusian State Pedagogical University named after M. Tank (Minsk, Belarus).

## FUNDING

This work was supported by the Abdus Salam International Center for Theoretical Physics (grant no. SMR 2424). The SPEM studies were performed within the project no. 20120120 at the ELETTRA synchrotron radiation source (ESCA station, Trieste, Italy).

## REFERENCES

1. J. Yamabe, T. Awane, and S. Matsuoka, Int. J. Hydrogen Energy **40**, 10329 (2015). https://doi.org/10.1016/j.ijhydene.2015.06.023
2. A. Kamegawa and M. Okada, Rev. High Pressure Sci. Technol. **17**, 173 (2007). https://doi.org/10.4131/jshpreview.17.173
3. P. Z. Zhao and T. Tsuchida, Mater. Sci. Eng., A **499**, 78 (2009). https://doi.org/10.1016/j.msea.2007.09.094
4. W. Qin and J. A. Szpunar, Philos. Mag. **97**, 3296 (2017). https://doi.org/10.1080/14786435.2017.1378451
5. J. R. Scully, G. A. Young, and S. W. Smith, in *Gaseous Hydrogen Embrittlement of Materials in Energy Technol-*

*ogies*, Ed. by R. P. Gangloff and B. P. Somerday (Woodhead, Cambridge, 2012), Vol. 1, p. 707.

6. M. Koyama, M. Rohwerder, C. C. Tasan, et al., Mater. Sci. Technol. **33**, 1481 (2017). https://doi.org/10.1080/02670836.2017.1299276
7. M. Asta, C. Beckermann, A. Karma, et al., Acta Mater. **57**, 941 (2009). https://doi.org/10.1016/j.actamat.2008.10.020
8. W. J. Boettinger and D. K. Banerjee, in *Physical Metallurgy,* Ed. by D. Laughlin and K. Hono, (Elsevier, Amsterdam, 2014), Vol. 1, p. 639.
9. E. Yu. Neumerzhitskaya and V. G. Shepelevich, Perspekt. Mater., No. 4, 69 (2005).
10. I. I. Tashlykova-Bushkevich, AIP Conf. Proc. **1697**, 090004 (2015). https://doi.org/10.1063/1.4937702
11. I. I. Tashlykova-Bushkevich, G. Itoh, V. G. Shepelevich, and T. Shikagawa, Mater. Trans. **52**, 895 (2011). https://doi.org/10.2320/matertrans.L-MZ201104
12. I. Tashlykova-Bushkevich, T. Shikagawa, T. Suzuki, V. Shepelevich, and G. Itoh, Mater. Sci. Forum **638–642**, 465 (2010). https://doi.org/10.4028/www.scientific.net/MSF.638-642.465
13. I. I. Tashlykova-Bushkevich and G. Itoh, in *ICAA13 Pittsburgh*, Ed. by H. Weiland, A. D. Rollett, and W. A. Cassada (Springer, Cham, 2012). https://doi.org/10.1007/978-3-319-48761-8_9
14. I. S. Miroshnichenko, *Quenching from the Liquid State* (Metallurgiya, Moscow, 1982) [in Russian].
15. L. Gregoratti, A. Barinov, E. Benfatto, et al., Rev. Sci. Instrum. **75**, 64 (2004). https://doi.org/10.1063/1.1630837
16. S. Günther, B. Kaulich, L. Gregoratti, and M. Kiskinova, Prog. Surf. Sci. **70**, 187 (2002). https://doi.org/10.1016/S0079-6816(02)00007-2
17. D. A. Shirley, Phys. Rev. B: Solid State **5**, 4709 (1972). https://doi.org/10.1103/PhysRevB.5.4709
18. NIST X-Ray Photoelectron Spectroscopy Database. https://srdata.nist.gov/xps/Default.aspx
19. SurfaceXplorer software. http://microtm.com/sx/sxr.htm
20. I. I. Tashlykova-Bushkevich, Yu. S. Yakovenko, V. G. Shepelevich, and I. S. Tashlykov, Fiz. Khim. Obrab. Mater., No. 3, 65 (2016).
21. I. I. Tashlykova-Bushkevich, M. Amati, B. Alemán, et al., Int. J. Hydrogen Energy **41**, 9100 (2016). https://doi.org/10.1016/j.ijhydene.2016.03.193
22. N. S. McIntyre, T. C. Chan, and C. Chen, Oxid. Met. **33**, 457 (1990). https://doi.org/10.1007/BF00666809
23. S. K. Kulkarni, M. G. Thube, and A. Nigavekar, Phys. Rev. B: Condens. Matter Mater. Phys. **37**, 6723 (1988). https://doi.org/10.1103/PhysRevB.37.6723
24. I. Ikemoto, K. Ishii, S. Kinoshita, et al., J. Solid State Chem. **17**, 425 (1976). https://doi.org/10.1016/S0022-4596(76)80012-6
25. M. Hassel, I. Hemmerich, H. Kuhlenbeck, and H.-J. Freund, Surf. Sci. Spectra **4**, 246 (1998). https://doi.org/10.1116/1.1247795
26. A. A. Tal, W. Olovsson, and I. A. Abrikosov, Phys. Rev. B **95**, 245402 (2017). https://doi.org/10.1103/PhysRevB.95.245402
27. E. P. Domashevskaya, S. V. Ryabtsev, V. A. Terekhov, et al., J. Struct. Chem. **52** (Suppl. 1), 115 (2011).
28. C. R. Henry, Surf. Sci. Rep. **31**, 231 (1998). https://doi.org/10.1016/S0167-5729(98)00002-8
29. V. D. Borman, M. A. Pushkin, V. N. Tronin, and V. I. Troyan, J. Exp. Theor. Phys. **110**, 1005 (2010). https://doi.org/10.1134/S1063776110060117
30. J. K. Parle, A. Beni, V. R. Dhanak, et al., Appl. Surf. Sci. **283**, 276 (2013). https://doi.org/10.1016/j.apsusc.2013.06.101
31. G. S. Frankel, A. J. Davenport, H. S. Isaacs, et al., J. Electrochem. Soc. **139**, 1812 (1992). https://doi.org/10.1149/1.2069503
32. O. Kubaschewski and B. E. Hopkins, *Oxidation of Metals and Alloys* (Butterworths, London, 1962; Metallurgizdat, Moscow, 1965).
33. I. I. Tashlykova-Bushkevich, Poverkhn.: Rentgenovskie, Sinkhrotronnye Neitr. Issled., No. 7, 105 (2010).
34. W. Zisman, in *Contact Angle, Wettability, and Adhesion*, Ed. by F. M. Fowkes (Am. Chem. Soc., Washington, DC, 1964), p. 1.
35. A.-M. Kietzig, M. N. Mirvakili, S. Kamal, et al., J. Adhes. Sci. Technol. **25**, 2789 (2011). https://doi.org/10.1163/016942410X549988
36. W. Liu, L. Sun, Y. Luo, et al., Appl. Surf. Sci. **280,** 193 (2013). https://doi.org/10.1016/j.apsusc.2013.04.124
37. P. Bizi-Bandoki, S. Benayoun, S. Valette, et al., Appl. Surf. Sci. **257,** 5213 (2011). https://doi.org/10.1016/j.apsusc.2010.12.089
38. C. Lee, H. Cho, D. Kim, and W. Hwang, Appl. Surf. Sci. **288**, 619 (2014). https://doi.org/10.1016/j.apsusc.2013.10.084
39. M. Rahimi, P. Fojan, L. Gurevich, and A. Afshari, Appl. Surf. Sci. **296**, 124 (2014). https://doi.org/10.1016/j.apsusc.2014.01.059
40. B. Lu and N. Li, Appl. Surf. Sci. **326**, 168 (2015). https://doi.org/10.1016/j.apsusc.2014.11.138
41. I. Tashlykova-Bushkevich, J. Yakovenka, I. Bushkevich, et al., Przegl. Elektrotech. **94**, 122 (2018). https://doi.org/10.15199/48.2018.04.30
42. A. Gajewski, Int. J. Heat Mass Transfer **51**, 4628 (2008). https://doi.org/10.1016/j.ijheatmasstransfer.2008.01.027
43. V. S. Rudnev, A. E. Lysenko, A. Yu. Ustinov, Prot. Met. Phys. Chem. Surf. **45**, 600 (2009). https://doi.org/10.1134/S2070205109050189
44. J. Elder, J. Cowie, and J. Weritz, Light Met. Age **75** (6), 20 (2017).
45. C. Zhang, P. Lv, H. Xia, et al., Vacuum **167**, 263 (2019). https://doi.org/10.1016/j.vacuum.2019.06.022
46. Y.-L. Su and Y.-F. Lin, Adv. Mech. Eng. (London, U. K.) **7** (6), 1 (2015). https://doi.org/10.1177/1687814015589721

*Translated by A. Tulyabaev*